Available online at www.sciencedirect.com
ScienceDirect
Journal of Power Sources 170 (2007) 520–526
JOURNAL OF POWER SOURCES
www.elsevier.com/locate/jpowsour

Influence of cobalt and manganese content on the dehydrogenation capacity and kinetics of air-exposed $LaNi_{5+x}$-type alloys in solid gas and electrochemical reactions

E. Raekelboom [a,*], F. Cuevas [a], B. Knosp [b], A. Percheron-Guégan [a]

[a] *Laboratoire de Chimie Métallurgique des Terres Rares CNRS, 2-8 rue Henri Dunant, 94320 Thiais, France*
[b] *SAFT, 111 bd. Alfred Daney, 33074 Bordeaux, France*

Received 18 January 2007; received in revised form 21 March 2007; accepted 5 April 2007
Available online 10 April 2007

Abstract

The effect of cobalt and manganese content on the dehydrogenation properties of air-exposed MmB_{5+x}-type (Mm = mischmetal; B = Ni, Al, Co and Mn) alloys was investigated both in solid gas and electrochemical reactions. The cobalt and manganese content were varied separately while keeping constant the plateau pressure of the hydrides. The increase of the cobalt content leads to a decrease of the hydrogen capacity whereas the manganese content has no much effect. In solid gas reactions, the kinetics were found to be limited by the hydrogen diffusion through the surface oxidation layer. As for the electrochemistry, the kinetics are limited by a corrosion layer formed in alkaline medium. The desorption rates for both processes increase as the cobalt or manganese content decreases. This is thought to be due to an enhancement of the hydrogen diffusivity through the oxidation layer. As a result, a low cobalt or manganese content in MmB_{5+x} alloys is found to be beneficial for the hydrogen desorption kinetics in both processes.

Keywords: Batteries; Kinetics; Intermetallics; Hydrogen storage materials; $LaNi_5$

1. Introduction

Ni-MH batteries are now widely used in portable applications such as phones and digital cameras. In these types of rechargeable batteries, the negative electrode is composed of MmB_{5+x}-type alloy (Mm = mischmetal; B = Ni, Al, Co and Mn) as active material which is derived from the binary $LaNi_5$ compound [1,2]. The nickel has been partially substituted by the manganese and aluminium in order to decrease the hydride plateau pressure below 0.1 MPa (0.17 MPa for $LaNi_5$ at 298 K) and by the cobalt which was found to increase the cycle life by reducing mainly the alloy decrepitation. Such a decrepitation is the result of strong internal stress due to a large volume expansion upon hydrogen uptake and release which exacerbates the corrosion of the electrode [3,4]. Owing to the high cost of cobalt, the initial content of ~10 wt.% was put down to 5 wt.% in commercialised batteries, whereas the stoichiometry of the alloys was increased up to a B/Mm ratio of 5.3. The overstoichiometry has a similar effect on the decrepitation than the cobalt content [5–7]. The mischmetal, being a cheaper mixture of rare earths, replaces the lanthanum.

Many works have been undertaken so far in order to estimate the influence of alloy chemical composition (i.e. B/Mm ratio, cobalt, manganese or aluminium content) on the capacity and cycle life. Overstoichiometric alloys have been shown to improve the cycling stability at the expense of their H-capacity [5,8]. Similar effect was observed for the cobalt, whose content superior of 5.6 wt.% was found to decrease the delivered capacity but increase its durability [8,9]. As for the manganese, its content was shown to have little effect on the capacity [10]. As far as the cycle-life is concerned, Mn substitution was found to be detrimental for stoichiometric alloys. For overstoichiometric ones, the cycle life passed through a maximum value for a specific manganese content [11].

Besides the capacity and the cycle life, an important property that the alloy must also have is the ability to deliver the capacity

* Corresponding author. Tel.: +33 321382788; fax: +33 169477697.
E-mail address: raekelboom@hotmail.com (E. Raekelboom).

0378-7753/$ – see front matter © 2007 Published by Elsevier B.V.
doi:10.1016/j.jpowsour.2007.04.003

in reasonable time according to the current required for the application. Can the composition influence the kinetics of the alloy? The question stayed unanswered since not trivial. The difficulty remains in the ability to look at the composition independently of the others parameters that could modify the kinetics, i.e. the decomposition hydride pressure and the alloy decrepitation. The aim of the present paper is to study the influence of the alloy composition, particularly the cobalt and manganese content, on both the desorption rates measured in solid gas phase and the high-rate dischargeability measured electrochemically. The study has been carried out with constant hydride plateau pressure, by varying the ratio La/Ce of the mischmetal. Overstoichiometric alloys were used in order to hinder the decrepitation phenomenon. In order to be coherent, both studies were undertaken respecting the same processing conditions prior to the kinetic measurements like the manual grinding of the alloy in air.

2. Experimental

2.1. Alloy preparation and characterisation

Six multi-substituted alloys of MmB_{5+x}-type (Mm = mischmetal; B = Ni, Al, Co and Mn) (see Table 1) with distinct Co and Mn contents, were melted in a vacuum induction furnace and annealed for 4 days at 1050 °C. In the Co-series, the cobalt content was varied in a domain between 0.37 and 0.72 atoms per formula unit (at. f.u.$^{-1}$), which corresponds to 4.9 and 9.5 wt.%, respectively. The stoichiometry and manganese content (B/Mm = 5.3; Mn = 0.4 at. f.u.$^{-1}$) was kept constant. In the Mn-series, the manganese takes values between 0.2 and 0.6 at. f.u.$^{-1}$ while keeping constant the stoichiometry and cobalt content (B/Mm = 5.2; Co = 0.55 at. f.u.$^{-1}$). For both series, the ratio of rare earth metals La/Ce was varied in order to keep a constant unit-cell volume. According to the geometrical law [12–14] which states that the logarithm of the plateau pressure linearly decreases with the unit-cell volume, this procedure should allow us to fulfil the constant plateau pressure condition. The alloys are labelled hereafter by a code according to the atomic composition of cobalt and manganese (see Table 1). The overstoichiometry x (MmB_{5+x}-type alloys) for the Co and Mn-series were fixed at 0.3 and 0.2, respectively, to minimise the decrepitation phenomenon even at low Co contents. The variation of the Co and Mn contents was counterbalanced by the Ni content to get the fixed stoichiometry. The alloys were characterised by Rietveld refinement of X-ray diffraction data (XRD) and electron probe microanalysis (EPMA). XRD measurements were performed in a Bruker AXS D8 θ–θ diffractometer equipped with Cu Kα radiation. EPMA analysis was done in a Cameca SX-100 instrument.

2.2. Pressure-composition isotherms and kinetics in solid gas phase

The pressure-composition isotherms (PCT) and kinetics have been measured at 45 °C using a Sieverts's type device. ~250 mg of air-ground alloy was sieved between 125 and 70 μm and introduced into a stainless steal sample holder that allows a good heat transfer. Such a holder is kept in a thermostatic bath. The variation of the alloy temperature during the reaction is considered to be limited due to the small quantity of alloy used, the good heat transfer and to the slow kinetics for air-ground alloys. PCT curves were obtained after an activation period of 10 cycles. For the kinetic measurement, a quasi-constant pressure method was used. The desorptions were conducted under an initial pressure of 8×10^{-3} MPa leading to a relative variation pressure $\Delta P_{des}/P_{des}$ of 40%. This variation has been taken into account and corrected for the kinetic analysis.

2.3. Electrochemical tests

Negative electrodes were prepared from a mixture of the powder alloy mechanically ground with carbon powder for conduction and a cellulosic thickener together with a styrene butadiene rubber binder into a nickel foam. The films were cut (2 cm × 2.5 cm) so that they contain ~1 g of alloy. The electrodes were cycled electrochemically *vs.* foam positive electrodes of $Ni(OH)_2$ and polyolefin separators soaked in a 8.7 M KOH electrolyte in a negative-limited open polyethylene electrochemical cell. The alloys were activated during the first 10 cycles during which the alloys were charged at C/10 for 16 h and discharged at

Table 1
Alloy composition, stoichiometry (B/A ratio), lattice parameters, unit-cell volume, desorption plateau pressures P_p (at 45 °C) and H-capacities (at 45 °C) for Co- and Mn-series

Code	Composition: targeted; measured by EPMA	B/A ratio: targeted; measured	Lattice parameter: a (Å); c (Å)	Cell vol. (Å^3)	P_p (MPa)	H (at. f.u.$^{-1}$)
Co0.73	$La_{0.69}Ce_{0.22}Nd_{0.07}Pr_{0.02}Ni_{3.88}Mn_{0.4}Al_{0.3}Co_{0.72}$; $La_{0.69}Ce_{0.22}Nd_{0.08}Pr_{0.01}Ni_{3.92}Mn_{0.41}Al_{0.27}Co_{0.73}$	5.3; 5.33(9)	5.0039(1); 4.0592(1)	88.022(4)	0.058	4.05
Co0.56	$La_{0.71}Ce_{0.20}Nd_{0.07}Pr_{0.02}Ni_{4.05}Mn_{0.4}Al_{0.3}Co_{0.55}$; $La_{0.71}Ce_{0.20}Nd_{0.08}Pr_{0.01}Ni_{4.11}Mn_{0.40}Al_{0.28}Co_{0.56}$	5.3; 5.35(6)	5.0057(1); 4.0556(1)	88.006(3)	0.059	4.94
Co0.37	$La_{0.72}Ce_{0.19}Nd_{0.07}Pr_{0.02}Ni_{4.23}Mn_{0.4}Al_{0.3}Co_{0.37}$; $La_{0.72}Ce_{0.19}Nd_{0.08}Pr_{0.01}Ni_{4.25}Mn_{0.39}Al_{0.30}Co_{0.37}$	5.3; 5.31(5)	5.0069(1); 4.0540(1)	88.016(4)	0.056	5.13
Mn0.55	$La_{0.34}Ce_{0.46}Nd_{0.15}Pr_{0.05}Ni_{3.75}Mn_{0.6}Al_{0.3}Co_{0.55}$; $La_{0.34}Ce_{0.46}Nd_{0.16}Pr_{0.04}Ni_{3.79}Mn_{0.56}Al_{0.31}Co_{0.56}$	5.2; 5.22(1)	4.9834(1); 4.0648(1)	87.425(3)	0.044	4.82
Mn0.40	$La_{0.57}Ce_{0.27}Nd_{0.12}Pr_{0.04}Ni_{3.95}Mn_{0.4}Al_{0.3}Co_{0.55}$; $La_{0.62}Ce_{0.25}Nd_{0.11}Pr_{0.02}Ni_{3.99}Mn_{0.40}Al_{0.28}Co_{0.55}$	5.2; 5.22(3)	5.0008(1); 4.0546(2)	87.816(3)	0.054	5.35
Mn0.20	$La_{0.83}Ce_{0.12}Nd_{0.04}Pr_{0.01}Ni_{4.15}Mn_{0.2}Al_{0.3}Co_{0.55}$; $La_{0.82}Ce_{0.12}Nd_{0.04}Pr_{0.02}Ni_{4.19}Mn_{0.20}Al_{0.31}Co_{0.55}$	5.2; 5.25(2)	5.0171(1); 4.0285(1)	87.818(4)	0.065	5.05

C/5 until 0.9 V versus $Ni(OH)_2$/NiOOH. The discharge rate R_m was evaluated as the reciprocal of the slope of the linear regression of the discharge capacity as a function of the discharge current. For the high rate dischargeability measurement, capacities were measured at room temperature using current densities of 1000 down to 50 mA g^{-1} after a charge at C/10 for 16 h.

3. Results and discussion

3.1. Alloy characterisation

All synthesized alloys are found to be single phase having a hexagonal structure (type $CaCu_5$, symmetry *P6/mmm*). Their composition, stoichiometry, lattice parameters and unit-cell volume are listed in the Table 1.

For the Co-series, the increase of the Co content, which is counterbalanced by Ni diminution, only demands a small decrease of the La/Ce ratio to keep a constant unit-cell volume. This results from the slightly larger atomic radius of Co as compared to that of Ni ($r_{Co} = 1.25$ Å; $r_{Ni} = 1.24$ Å) which is compensated by the smaller atomic radius of Ce as compared to that of La ($r_{La} = 1.87$ Å; $r_{Ce} = 1.81$ Å). As sought, the unit-cell volumes are almost identical ($V \sim 88.01$ Å^3), whereas an anisotropic behaviour of the lattice parameters is observed. On increasing the Co content, the *a* parameter decreases slightly whereas the *c* parameter increases.

For the Mn-content, the increase of the Mn content requires a high decrease of the La/Ce ratio. This results from the much larger atomic radius of Mn ($r_{Mn} = 1.35$ Å) as compared to that of Ni. The unit-cell volumes are, however, smaller than for the Co-series ($V \sim 87.82$ Å^3), particularly at high Mn-content ($V = 87.425$ Å^3 for the Mn0.55 alloy). As far as the lattice parameters are concerned, the anisotropic effect is again observed but with much higher intensity: on increasing the Mn content, the *a* parameter decreases whereas the *c* parameter increases. As shown by Qingxue et al. [15] the increase of the La/Ce ratio yields a strong increase of the *a* parameter and a small decrease of the *c* parameter due to close packing geometry of the hexagonal lattice. Besides, some additional anisotropy can be induced by the nature of the atoms that occupy the dumbbell sites in over-stoichiometric alloys. The dumbbells in Mn-rich overstoichiometric alloys consist mainly of two Mn atoms [11]. On increasing the Mn-content, Mn-atoms will preferently populate the dumbbells with an extra increase of the *c* parameter.

3.2. Pressure composition isotherms

The desorption PCT curves are given in Fig. 1 (Co-series) and Fig. 2 (Mn-series). The capacities were found to decrease from 5.13 to 4.05H f.u.$^{-1}$ when the Co content increases from 0.37 to 0.73 at. f.u.$^{-1}$ (Fig. 1). This Co effect has been already reported in the literature [8]. The plateau pressures lay around 0.058 MPa in both absorption (not shown for clarity) and desorption, as no hysteresis was observed.

As for the manganese, the capacity increases first from 5.05 up to 5.35 H f.u.$^{-1}$ when the Mn content increases from 0.2 to 0.4 at. f.u.$^{-1}$ and then decreases down to 4.82 H f.u.$^{-1}$ for a, Mn content equal to 0.55 at. f.u.$^{-1}$ (Fig. 2). Contrary to the cobalt, the manganese content has less effect on the capacity. No hysteresis is observed between the absorption and desorption isotherms. The plateau pressures decrease from 0.065 to 0.044 MPa as the Mn content increases from 0.2 to 0.55 at. f.u.$^{-1}$ (Fig. 3). Such a decrease is unexpected since it does not obey the Lundin's empirical law which states that the logarithm of plateau pressure linearly decreases with the unit-cell volume. The origin of this anomaly is at present unknown. The Fig. 3 gathers the relationship between plateau pressures and the unit-cell volumes for both Co and Mn-series. The pressures stay close to a mean value of 0.058 MPa.

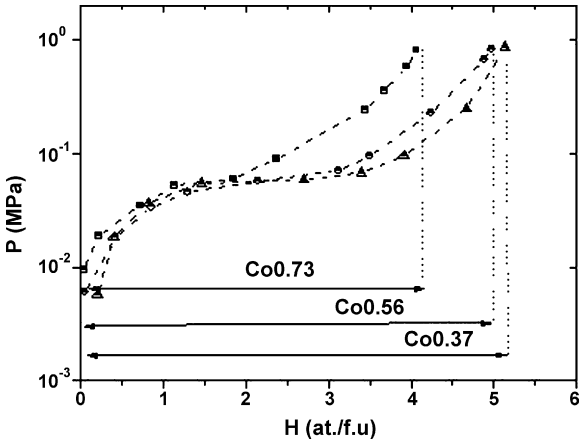

Fig. 1. Pressure composition desorption isotherms at 45 °C for the Co0.37, Co0.56 and Co0.73 alloys after 10 absorption/desorption cycles.

3.3. Desorption rates in solid gas phase

The rates of the solid-gas reaction can be written as $d\delta/dt = kF(P)G(\delta)$ [16] where δ is the reacted fraction (ratio between desorbed hydrogen at a given time and total hydrogen content), $F(P)$ the rate dependence on the hydrogen pressure, $G(\delta)$ the rate dependence on the alloy reacted fraction and k, the reaction rate constant. The pressure dependence function $F(P)$ was determined in order to take into account the large pressure

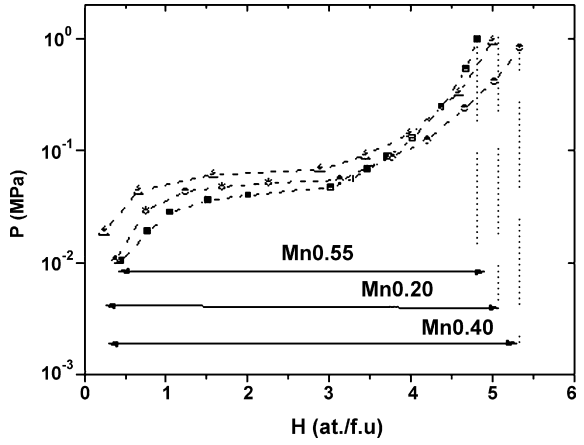

Fig. 2. Pressure composition desorption isotherms at 45 °C for the Mn0.2, Mn0.40 and Mn0.55 alloys at 45 °C after 10 absorption/desorption cycles.

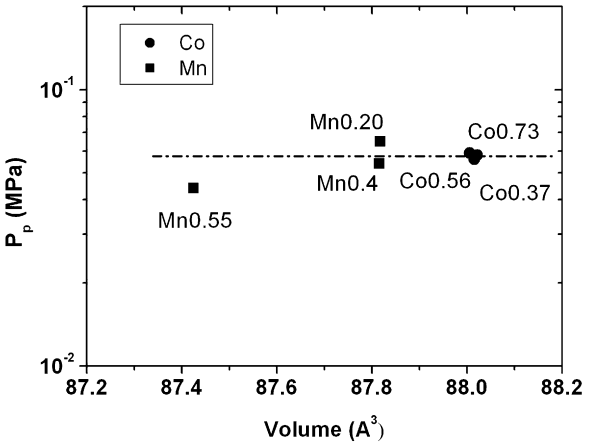

Fig. 3. Decomposition plateau pressures P_p of the hydrides at 45 °C as a function of the alloy unit-cell volume for both cobalt and manganese series. Dashed line stands for the average value of 0.058 MPa.

variation ($\Delta P_{des}/P_{des} \sim 40\%$) that occurs during the desorption. To this aim, the initial desorption pressure was varied within the range 4–12 × 10^{-3} MPa. As an exemple, Fig. 4 shows the effect of the pressure P on the desorption rates at $\delta = 0.5$ for Mn0.4 alloy. The plots yield good straight lines suggesting that $F(P)$ takes the form of $\ln(P_p/P)$ where P_p is the plateau pressure. In the following results, this correction has been applied on the desorption rates for all the alloys.

The desorption rates $d\delta/dt$ collected after an activation period of ten cycles are shown at Fig. 5 for the cobalt and manganese series against the reacted fraction δ. There are several possible steps that could be rate determining during the desorption: (1) hydride decomposition at the hydride/intermetallic interface, (2) bulk diffusion within hydride and intermetallic phases, (3) bulk to surface transfer or (4) recombination and desorption to the gas phase. For a given rate limiting step, the dependence of the rate on the reacted fraction will be different. As shown in Fig. 5, the desorption rates for all alloys decrease asymptotically toward zero indicating a diffusion phenomenon to be the rate limiting

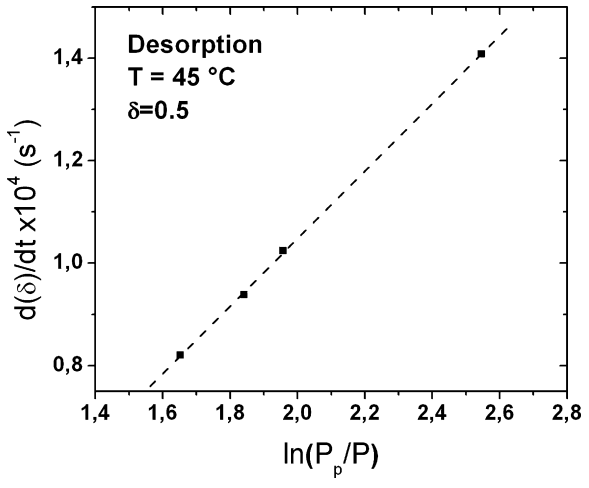

Fig. 4. Dependence of the desorption rates, $d\delta/dt$ at $\delta = 0.5$ on the pressure function $\ln(P_p/P)$ for the Mn0.4 alloy ($P_p = 5.4 \times 10^{-2}$ MPa). Dashed line is the best linear fit to the measured points.

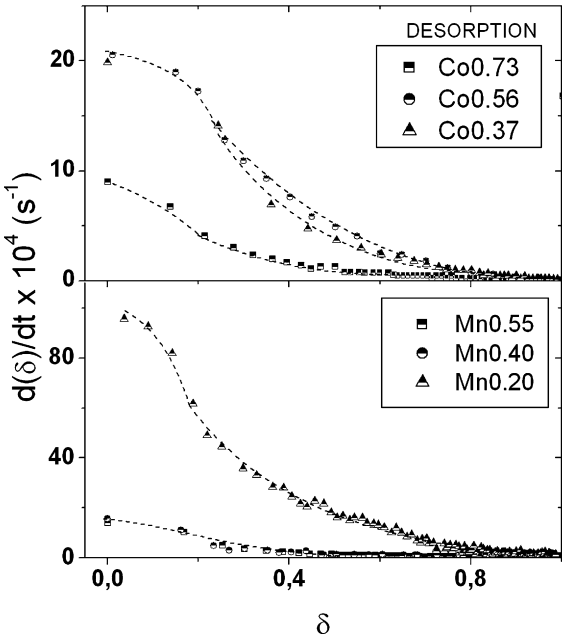

Fig. 5. Evolution of the desorption rates with the reacted fraction δ for both Co- and Mn-series.

step [17]. Furthermore, if we compare the kinetics of currently air-exposed Mn0.4 with the same alloy ground in argon (Fig. 6), we see that the time to release 80% of the hydrogen is divided by 100 when the alloy is ground in Ar. The slower desorption kinetics measured for the alloys kept in air is due to the formation of an oxidation layer at the surface of the alloys throughout which the hydrogen diffuses. The existence of such oxide layer has been confirmed by TEM measurements. The composition of the oxidation layer formed in air has not been determined here specifically but previous studies have shown they were made of Mm_2O_3, nickel rich alloy and $NiMm_2O_4$ [18].

For air ground alloys, the times needed to release 80% of the hydrogen versus the number of cycles are shown at Fig. 7. The plots show a decrease of the desorption times on the first five cycles, called activation period, till they stabilize. Final desorption times are much longer than for argon-grinded alloys,

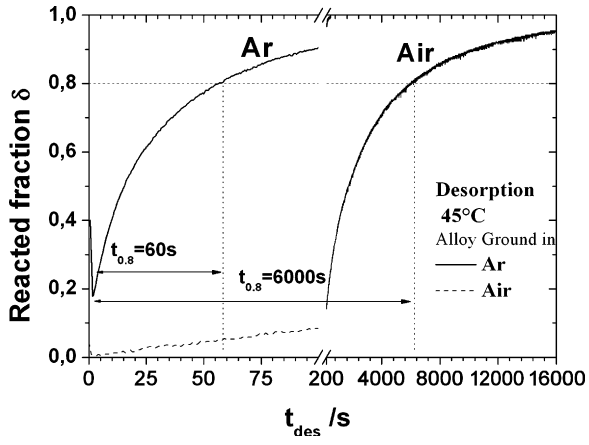

Fig. 6. Time-evolution of the reacted fraction for the Mn0.4 alloy ground either in air or argon atmosphere.

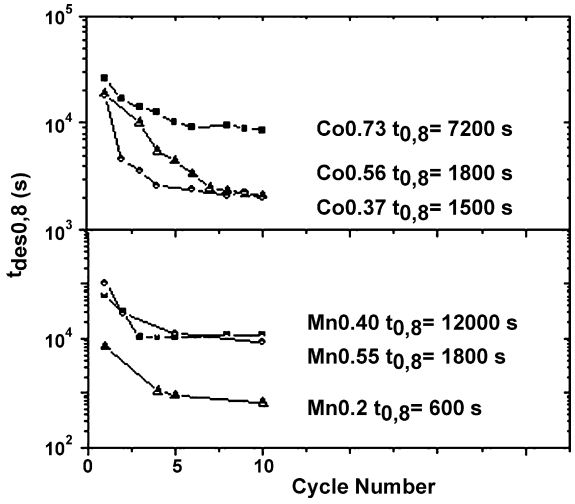

Fig. 7. Evolution for both Co-and Mn-series of the desorption time $t_{des0.8}$ to attain a reacted fraction of 0.8 with the number of cycles.

suggesting that no fresh alloy surfaces are created upon hydrogenation cycling. As can be observed in Fig. 8, the lack of alloy decrepitation on cycling has been confirmed by SEM observations of both gas and electrochemical cycling. The activation period is therefore attributed to minor modifications of the oxide layer on cycling.

Fig. 9 shows the evolution, after ten activation cycles, of the desorption rates at $\delta = 0.5$ with both cobalt and manganese contents. For both series, the desorption rates exhibit a tendency to decrease on increasing both Co- and Mn-contents.

3.4. Electrochemical characterisation

The electrochemical capacities were measured for the two series while varying the discharge current. As a first approximation, the capacity delivered by the alloy decreases linearly as the current increases due to the finite kinetics of hydrogen discharge resulting in concentration polarization (Fig. 10). This causes a drop in cell voltage, which results in termination of the discharge before the maximum capacity of the electrode is recovered. From Fig. 10, several parameters can be extracted and compared. The maximum discharge rate R_m, which is the

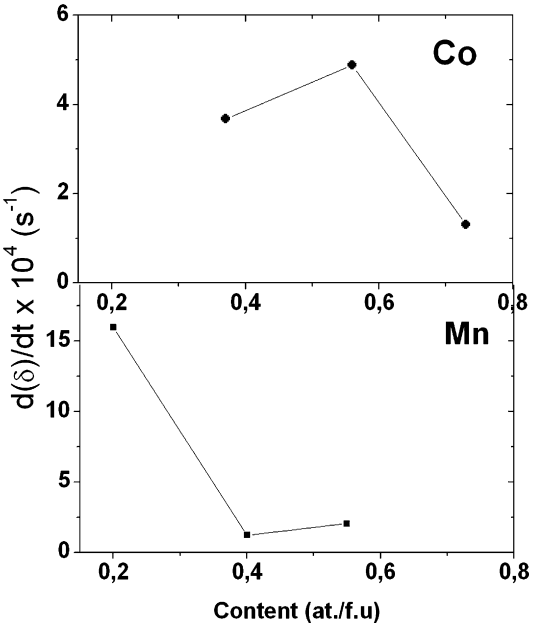

Fig. 9. Evolution of the desorption rates at $\delta = 0.5$ with cobalt and manganese contents.

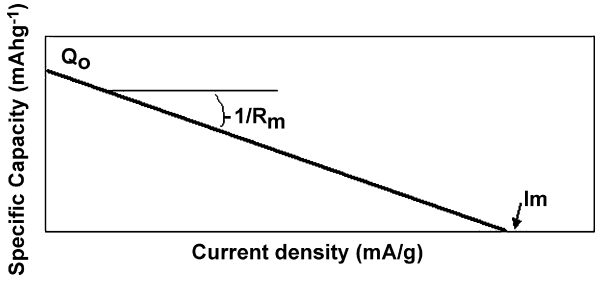

Fig. 10. Typical dependence of the specific capacity with the current density in an electrochemical cell. R_m is the maximum discharge rate, Q_0 the maximum capacity and I_m is the maximal discharge current.

reciprocal of the slope of the linear plot, is defined by the ratio I_m/Q_0, where Q_0 is the the maximum capacity (obtained by extrapolation toward the infinitesimal value of the current) and I_m is the maximal discharge current (obtained by extrapolation

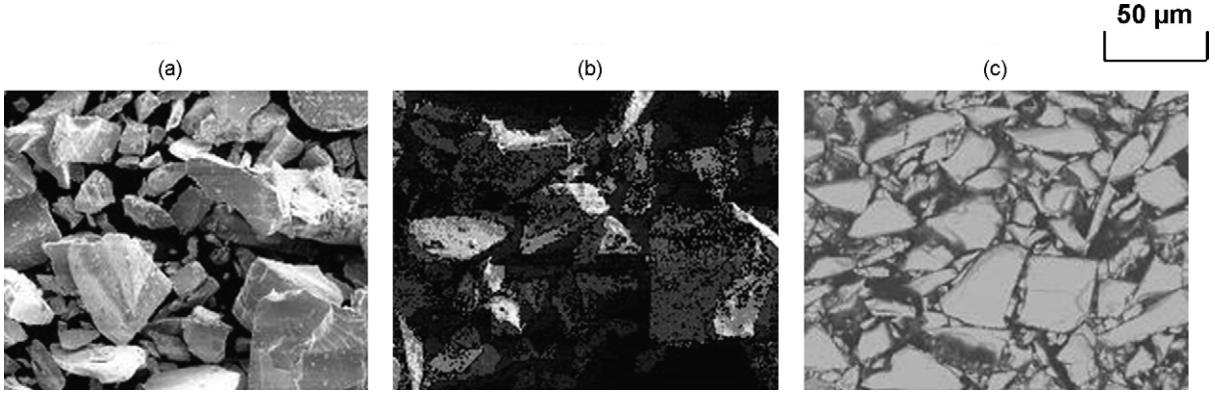

Fig. 8. SEM images of a representative alloy (Co0.37) before (a) and after both gas (b) and electrochemical cycling (c).

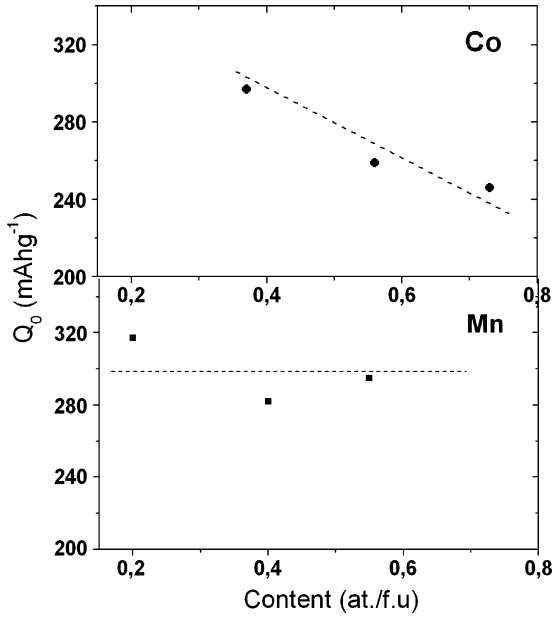

Fig. 11. Evolution of the maximum capacity Q_0 with cobalt and manganese contents. Dashed lines are the best linear fit to the measured points.

toward the infinitesimal value of the capacity). Q_0 and I_m are useful to predict the time, t_{app}, that a battery can withstand at a required discharge current, I_{app}. These parameters are linked by the equation:

$$I_{app} = \frac{Q_0}{t_{app} + 1/R_m}$$

Furthermore, this equation states that, when comparing different alloys, the one with the highest rate R_m will provide the highest discharge current, I_{app}, for a given Q_0 and discharge time.

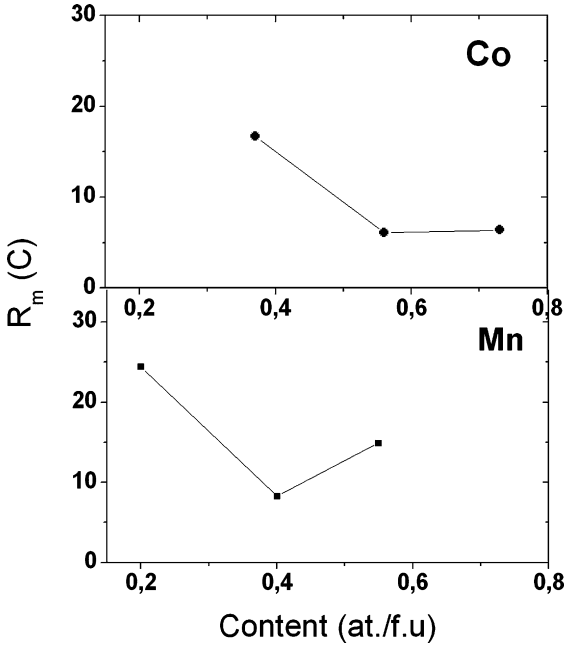

Fig. 12. Evolution of the maximum discharge rate R_m with cobalt and manganese contents.

The maximum capacities Q_0 for cobalt and manganese series are shown at Fig. 11. For the Co-series, the delivered capacities decrease as the cobalt content increases. On the contrary, the capacities do not vary much with the manganese content. Therefore, similar with results are obtained for both solid-gas and electrochemical measurements.

The values of R_m for Co- and Mn-series are shown in Fig. 12. In the first case, the values of R_m decrease when the cobalt content increases from 0.37 to 0.56 at. f.u.$^{-1}$ and then remains constant, whereas for the manganese it shows a minimum value for intermediate manganese content, i.e. for Mn0.4. Nevertheless, as a general trend, slower kinetics are observed in both solid-gas and electrochemical measurements on increasing cobalt and manganese contents.

4. Discussion

Our electrochemical measurements do not permit to determine the limiting step that controls the discharging kinetics. The situation is not trivial since there are several parameters that could play a role on the electrochemical kinetics. These are mainly the composition of the alloys (if the kinetics are limited by bulk hydrogen diffusion) and the composition and thickness of the corrosion layer formed in contact with the electrolyte (in a case of a limitation by charge transfer or hydrogen diffusivity through the surface corrosion layer) [19,20]. Since no decrepitation is observed on cycling (see Fig. 8), particle size variation is excluded to influence the measured electrochemical kinetics.

The maximum discharge rates R_m are between 6 C and 25 C which corresponds to typical discharging times of 600 s and 144 s, respectively. For Mn0.4 alloy, the electrochemical discharge time is 430 s. As compared to solid-gas reaction (Fig. 3), this value is lower than the typical desorption times found for air-grinded alloy (6000 s) but still higher than for the Ar-grinded alloy (60 s). This can be explained by the removal, upon electrochemical cycling, of the original oxide layer and the formation of a more permeable corrosion layer due to KOH soaking. Such a layer is known to be composed of a metallic solid solution (Ni, Co), oxide solid solution (Ni, Co)O and mischmetal hydroxide [18]. This layer may control the kinetics by limiting either hydrogen penetration or charge transfer reaction at the surface electrode particles. Thus, longer discharge times are obtained for electrochemical as compared to solid-gas reaction for Ar-grinded alloy. However, we cannot draw a definite conclusion, since the faster kinetics for the latter can be also due to the higher reaction temperature (45 °C) in solid-gas measurements.

Both Co- and Mn-series provide slower kinetics when the content of both elements increases. Since the kinetics seem to be controlled by the diffusion through the corrosion layer, the content of this layer in both elements turns to be a key factor. It could be argued that nickel, whose content in the studied alloys decreases as cobalt or manganese increases, might also have a beneficial effect on the kinetic. Nickel is considered to be a good electrocatalyst improving the charge transfer kinetics at the electrode surface [21]. However, in a previous study on the

effect of the alloy stoichiometry on the desorption rates [22], we have shown that the electrode discharging rates (i.e. R_m) do not depend on the alloy nickel content. In the light of these results, we believe that the electrochemical kinetics is not limited by the charge transfer reaction but, much probably, by the hydrogen diffusivity through the corrosion layer. Such diffusivity would be highly dependent on the Co- and Mn-content in the corrosion layer.

5. Conclusion

Dehydrogenation kinetics have been studied in air-exposed $LaNi_{5+x}$-type alloys while varying the cobalt and manganese content independently of the hydride decomposition pressure and the decrepitation. In order to achieve a constant plateau pressure, the increase of cobalt and manganese contents was accompanied by a decrease of the La/Ce ratio and Ni content. For both series, the oxide formation at the surface in air-exposed alloys leads to slower kinetics compared with alloys handled under argon atmosphere. The diffusion of hydrogen through the oxide layer is thought to be the rate limiting step in solid-gas reaction experiments. In these experiments, the increase of both cobalt and manganese contents leads to slower kinetics. The electrochemical discharge rates, R_m, are also found to decrease as the cobalt or manganese increases below values of 0.56 and 0.40 at. f.u.$^{-1}$, respectively. These last results are thought to originate from an intrinsic effect of the cobalt or manganese on the diffusivity of hydrogen through the electrolytically formed corrosion layer.

Acknowledgements

Authors would to thank the French Ministry of Research for the financial support, J.-L. Pastol, E. Leroy and B. Decamps for respectively the SEM, EPMA and TEM analysis.

References

[1] J.J.G. Willems, Philips J. Res. Suppl. 39 (1) (1984) 10.
[2] J.R.G.C.M. van Beek, J.J.J.G. Willems, H.C. Donkerslock, in: L.J. Pearce (Ed.), Proceedings of the 14th International Power Sources Symposium, Brighton, Power Sources 10 (1985) 317.
[3] T. Sakai, K. Oguro, H. Miyamura, N. Kuriyama, A. Kato, H. Ishikawa, C. Iwakura, J. Less-Common Met. 161 (1990) 193.
[4] G.D. Adzic, J.R. Johnson, S. Mukerjee, J.M. Breen, J.J. Reilly, J. Alloys Compd. 253/254 (1997) 579.
[5] P.H.L. Notten, R.E.F. Einerhand, J.L.C. Daams, J. Alloys Compd. 210 (1994) 221.
[6] P.H.L. Notten, R.E.F. Einerhand, J.L.C. Daams, J. Alloys Compd. 231 (1995) 604.
[7] M. Latroche, P.H.L. Notten, A. Percheron-Guégan, J. Alloys Compd. 253/254 (1997) 295.
[8] J.J. Reilly, G.D. Adzic, J.R. Johnson, T. Vogt, S. Mukerjee, J. McBreen, J. Alloys Compd. 293/294 (1999) 569.
[9] T. Sakai, K. Oguro, H. Miyamura, H. Kiriyama, A. Kato, H. Ishikawa, J. Less-Common Met. 161 (1990) 193.
[10] C. Lartigue, A. Percheron-Guégan, J.C. Achard, F. Tasset, J. Alloys Compd. 75 (1980) 23.
[11] P.H.L. Notten, M. Latroche, A. Percheron-Guégan, J. Electrochem. Soc. 146 (1999) 3181.
[12] J.-C. Achard, A. Percheron-Guégan, H. Diaz, F. Briaucourt, F. Demany, Proceedings of the Second International Congress on Hydrogen in Metals, Paris, 1977, p. 1E12.
[13] M.H. Mendelsohn, D.M. Gruen, A.E. Dwight, Nature 269 (1977) 45.
[14] C.E. Lundin, F.E. Lynch, C.B. Magee, J. Less-Common Met. 56 (1977) 19.
[15] Z. Qingxue, J.-M. Joubert, M. Latroche, D. Jun, A. Percheron-Guégan, J. Alloys Compd. 360 (2003) 290.
[16] P.D. Goodell, P.S. Rudman, J. Less-Common Met. 89 (1983) 117.
[17] C. Park, J. Lee, J. Less-Common Met. 91 (1983) 189.
[18] F. Maurel, B. Knosp, M. Backhaus-Ricoult, J. Electrochem. Soc. 147 (1) (2000) 78.
[19] H.J. Van Rijswick, in: A.F. Andresen, A.J. Maeland (Eds.), Hydrides for Energy Storage, Pergamon Press, Oxford, England, 1978, p. 261.
[20] X. Yuan, N. Xu, J. Electrochem. Soc. 149 (4) (2002) A407.
[21] P.H.L. Notten, P. Kokkeling, J. Electrochem. Soc. 138 (7) (1991) 1877.
[22] E. Raekelboom, F. Cuevas, B. Knosp, A. Percheron-Guégan, J. Alloys Compd. 404–406 (2005) 347.